H. Hasegawa[1], R. E. Denton[2], T. K. M. Nakamura[3], K. J. Genestreti[4], T. D. Phan[5], R. Nakamura[6], K.-J. Hwang[7], N. Ahmadi[8], Q. Q. Shi[9], M. Hesse[10], J. L. Burch[7], J. M. Webster[7], R. B. Torbert[4,11], B. L. Giles[12], D. J. Gershman[12], C. T. Russell[13], R. J. Strangeway[13], H. Y. Wei[13], P.-A. Lindqvist[14], Y. V. Khotyaintsev[15], R. E. Ergun[16], and Y. Saito[1]

[1]Institute of Space and Astronautical Science, Japan Aerospace Exploration Agency, Sagamihara, Japan.

[2]Department of Physics and Astronomy, Dartmouth College, Hanover, NH, USA.

[3]Institute of Physics, University of Graz, Graz, Austria.

[4]Southwest Research Institute, Durham, NH, USA.

[5]Space Sciences Laboratory, University of California, Berkeley, CA, USA.

[6]Space Research Institute, Austrian Academy of Sciences, Graz, Austria.

[7]Southwest Research Institute, San Antonio, TX, USA.

[8]Laboratory for Atmospheric and Space Physics, University of Colorado, Boulder, CO, USA.

[9]Shandong Provincial Key Laboratory of Optical Astronomy and Solar-Terrestrial Environment, Institute of Space Sciences, Shandong University, Weihai, China.

[10]Space Plasma Physics Group, University of Bergen, Bergen, Norway.

[11]Physics Department, University of New Hampshire, Durham, NH, USA.

[12]NASA Goddard Space Flight Center, Greenbelt, MD, USA.

[13]Department of Earth, Planetary, and Space Sciences, University of California, Los Angeles, CA, USA.

[14]Royal Institute of Technology, Stockholm, Sweden.

[15]Swedish Institute of Space Physics, Uppsala, Sweden.

[16]Department of Astrophysical and Planetary Sciences, University of Colorado, Boulder, CO, USA.

Corresponding author: Hiroshi Hasegawa (`hase@stp.isas.jaxa.jp`)

Key Points:

- Multispacecraft observations consistent with magnetic field annihilation in an electron diffusion region (EDR) of magnetotail reconnection
- Fully kinetic simulation of antiparallel magnetic reconnection shows that fast magnetic field annihilation can occur in an elongated EDR

- Theoretical analysis suggests fast collisionless magnetic diffusion in the elongated portion of EDR with nongyrotropic electrons

Abstract

We present observations in Earth's magnetotail by the Magnetospheric Multiscale spacecraft that are consistent with magnetic field annihilation, rather than magnetic topology change, causing fast magnetic-to-electron energy conversion in an elongated electron-scale current sheet. This energy conversion process is in contrast to that in the standard electron diffusion region (EDR) of a reconnecting current sheet where the energy of antiparallel magnetic fields is mostly converted to electron bulk-flow energy. Fully kinetic simulation also demonstrates that an elongated EDR is subject to the formation of electron-scale magnetic islands in which fast energy conversion is dominated by the annihilation. Consistent with the observations and simulation, theoretical analysis shows that fast magnetic diffusion can occur in an elongated EDR in the presence of nongyrotropic electron effects. The discovery of the annihilation-dominated EDR reveals a new form of energy conversion in the collisionless reconnection process.

Plain Language Summary

Magnetic reconnection in electric current sheets is the key to fast release of magnetic energy in many space and astrophysical plasma systems, such as during magnetospheric substorms and solar flares. Establishing the mechanism by which magnetic energy is converted to particle energy in the reconnection process is the key to understanding the large-scale impacts of reconnection, including energy partition and particle acceleration. It is generally believed that an electron-scale diffusion region (EDR), where a magnetic-to-electron energy conversion occurs, has an X-type magnetic field geometry around which the energy of antiparallel magnetic fields injected into the EDR is mostly converted to the bulk-flow energy of electrons by magnetic tension of reconnected field lines. Contrary to this standard X-type magnetic field geometry of reconnection, we report observations in Earth's magnetotail by NASA's Magnetospheric Multiscale spacecraft showing that the EDR can be highly elongated. The important and surprising consequence of the observed elongated shape of the EDR is that the fast energy conversion in the EDR is caused mostly by magnetic field annihilation, rather than magnetic topology change. The fast collisionless annihilation that we discovered is fundamentally different from the classical magnetic field annihilation due to collisional and wave-induced resistivity.

1 Introduction

Magnetic reconnection in Earth's magnetotail is fast, with an inflowing plasma speed of ~0.1 times the Alfvén speed in the inflow region, and has large-scale impacts, for example, explosive release of magnetic energy during magnetospheric substorms (Angelopoulos et al., 2008; Nagai et al., 2011). Magnetotail reconnection occurs under such simple boundary conditions that on the two sides of the current sheet the magnetic field is approximately oppositely-directed with

a comparable intensity, and plasmas have similar densities and temperatures. Such nearly antiparallel and symmetric reconnection is ideal for studying intrinsic properties of magnetic reconnection in the collisionless regime.

In the standard model of reconnection, the electron diffusion region (EDR), where both ions and electrons violate the 'frozen-in condition', is localized with an X-type field geometry where a magnetic-to-electron energy conversion occurs by changing the magnetic field topology (Torbert et al., 2018) (Figure 1a). It is generally accepted that in such EDRs most of the energy of antiparallel magnetic fields injected by the inflow is converted to bulk-flow energy of electrons ejected into the regions downstream of the EDR (Shay et al., 2007), called the exhausts, by magnetic tension (Lorentz force) of reconnected field lines. Numerical simulations suggest that the EDR may be elongated to a planar geometry (Figure 1b), resulting in a reduction of the reconnection rate (Daughton et al., 2006; Fujimoto, 2006). An elongated EDR is subject to the formation of electron-scale magnetic islands, in and around which significant energy conversion may persist through magnetic field annihilation (Text S6; Nakamura et al., 2021) (Figure 1e,f). However, there has been a lack of observations to understand if and how fast energy conversion occurs in such spatially extended EDRs with negligibly small reconnected field components across the current sheet. This is not only because unambiguous identification of EDR structures in space requires high-spatiotemporal-resolution plasma measurements, but also because there has been no data analysis method to distinguish whether the magnetic field injected into the EDR is reconnected or annihilated.

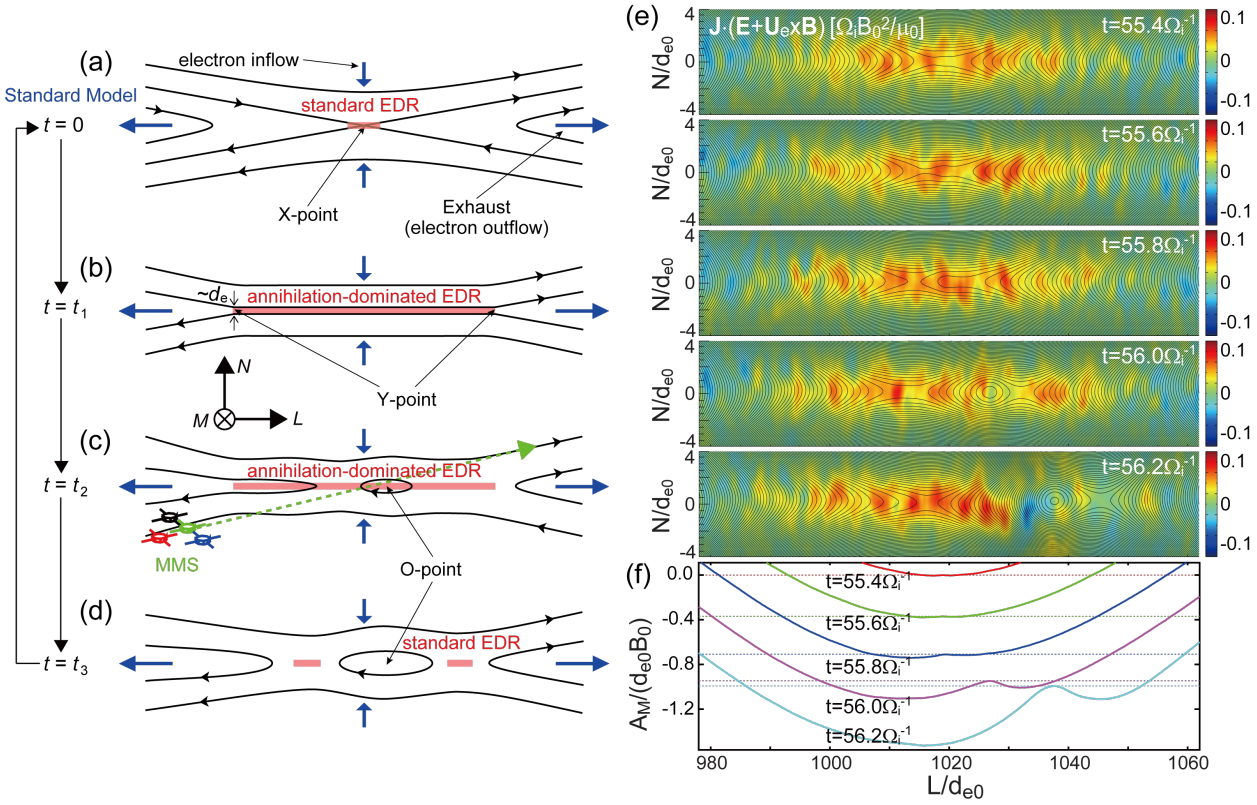

Figure 1. Possible sequence of time evolution of the electron-scale current sheet observed by MMS on 10 August 2017, and simulated EDR evolution. (a) Standard EDR with an X-type magnetic field geometry where the magnetic-to-particle energy conversion is mostly due to magnetic topology change (Torbert et al., 2018). (b) EDR after elongation along L, as seen in kinetic simulations (Daughton et al., 2006), where the energy conversion may be mostly due to magnetic field annihilation (Text S7 in the Supporting Information; see also Nakamura et al., 2021). (c) Initial stage of the magnetic island formation in the EDR, as observed by MMS. (d) Possible later stage of the island growth in exhausts of the EDRs. (e) Time evolution of an EDR from a fully kinetic simulation of turbulent reconnection (Nakamura et al., 2021), showing EDR elongation and island growth. In-plane magnetic field lines are shown by black curves and energy conversion rate $\mathbf{j} \bullet (\mathbf{E} + \mathbf{v}_e \times \mathbf{B})$ (Zenitani et al., 2011) in color, where $\mathbf{E}$ and $\mathbf{B}$ are the electric and magnetic fields, respectively, $\mathbf{j}$ current density, and $\mathbf{v}_e$ electron flow velocity. (f) Simulated vector potential (flux function) A_M along $N = 0$ for selected times. It shows that A_M at the O-point (local A_M maximum) continuously decreases from $t = 55.6\Omega_i^{-1}$ to $56.0\Omega_i^{-1}$ at a rate comparable to that at the primary X-point (A_M minimum), where Ω_i is ion gyrofrequency, demonstrating that magnetic field annihilation occurs in and around the island (Text S6).

In this letter, we present in-depth analysis of the fortuitous multi-spacecraft observations by the Magnetospheric Multiscale (MMS) mission (Burch et al., 2016) of a magnetotail EDR on 10 August 2017 (Zhou et al., 2019), in which the magnetic-to-particle energy conversion rate was consistent with fast reconnection. Contrary to the standard model of reconnection with an X-type field geometry at the EDR, however, our analysis suggests that the EDR was elongated in the outflow direction and the fast energy conversion observed in the EDR was supported by magnetic field annihilation, rather than magnetic topology change. Consistent with this interpretation, our theoretical analysis shows that fast magnetic diffusion can occur in an elongated EDR in the presence of nongyrotropic electron effects.

2 Overview of the Observations

In Figures 2a-2d, we show the context of the reconnecting current sheet observed by the MMS 2 spacecraft on 10 August 2017 at 12:17:40–12:19:40 UT, when MMS was fully embedded in the hot magnetotail plasma sheet (Zhou et al., 2019) at $(-15.2,\ 4.6,\ 3.1)\ R_E$ in GSM coordinates. The current sheet at 12:18:30 UT is characterized by a reversal from anti-sunward to sunward ion flows (negative to positive v_{ix} change in Figure 2b), crossing from its southern to northern side (negative to positive B_x change in Figure 2a). The ion flow speeds around the start and end of the interval are comparable to the ion Alfvén speed $V_{\rm iA} = \frac{B}{(\mu_0 \rho)^{\frac{1}{2}}} \approx 850$ km s^{-1} based on the magnetic field intensity $B \approx 15$ nT and proton number density of 0.15 cm^{-3}, where μ_0 is the vacuum permeability and ρ is plasma mass density. A fast dawnward electron flow ($v_{ey} \approx -10$ Mm s^{-1} in Figure 2c) and a relatively slow duskward ion flow with no enhancement at the current sheet show that its electric current was supported by electrons. These features indicate that MMS crossed an electron-scale current sheet (ECS) embedded inside a region of large-scale reconnection when traversing from its anti-sunward exhaust to sunward exhaust. Earlier studies of this current sheet (Zhou et al., 2019; Li et al., 2019) reported established signatures of EDRs (Burch et al., 2016; Torbert et al., 2018), including oppositely-directed electron jets with a speed exceeding $V_{\rm iA}$ (Figure 2c), crescent-shaped electron velocity distributions, and magnetic-to-particle energy conversion.

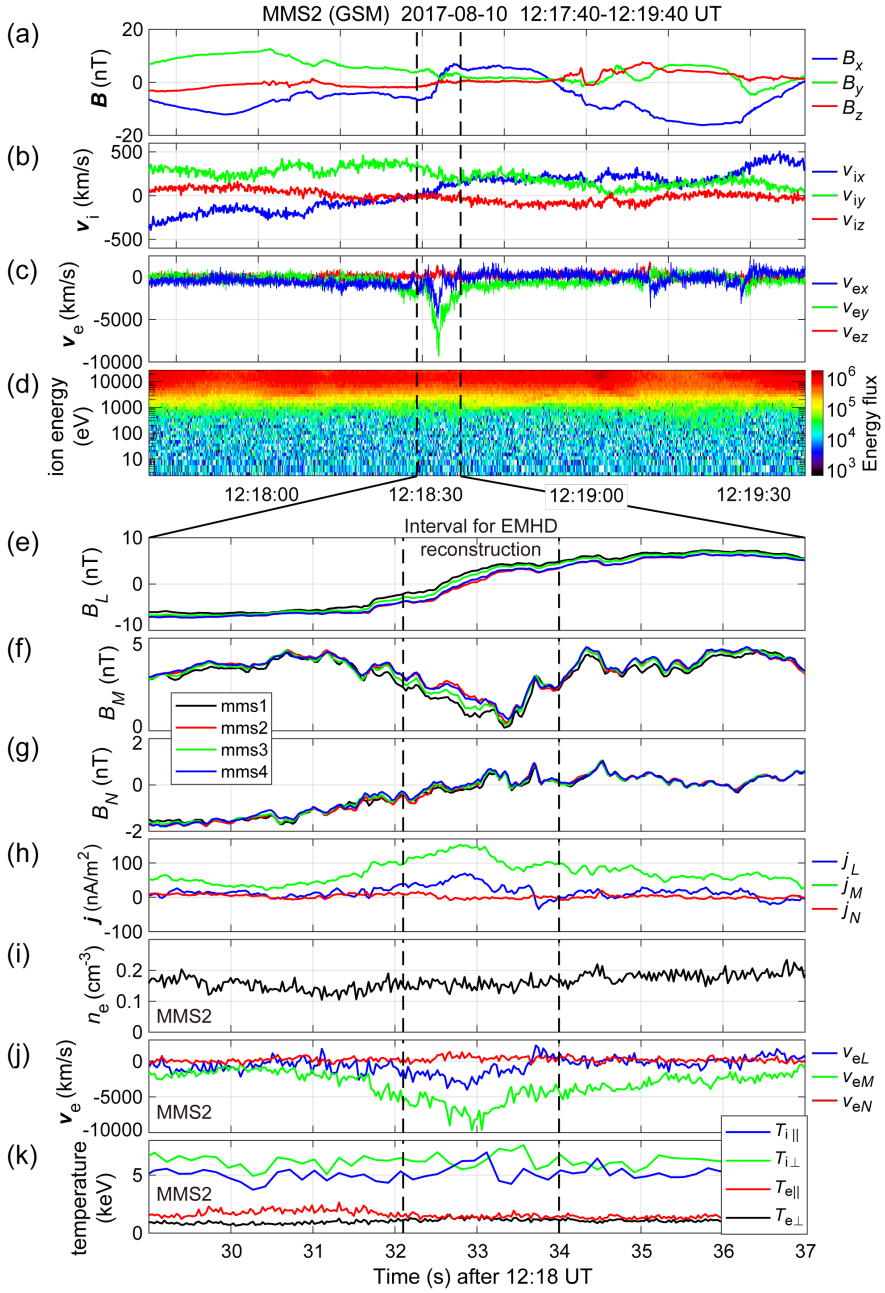

Figure 2. Overview of MMS observations of an electron-scale current sheet with both ion and electron reconnection jet signatures. (a-d) GSM components of the magnetic field (a; B_x, B_y and B_z), ion velocity (b; v_{ix}, v_{iy} and v_{iz}), electron velocity (c; v_{ex}, v_{ey} and v_{ez}) and ion energy-time spectrogram of omni-

directional differential energy flux (d; color scale, in units of keV s^{-1} cm^{-2} sr^{-1} keV^{-1}) seen by MMS 2. (e-h) Components in a common current-sheet (LMN) coordinate system of the magnetic field (e-g; B_L, B_M and B_N) from all four spacecraft (black, MMS 1; red, MMS 2; green, MMS 3; blue, MMS 4) and current density $\mathbf{j}=\frac{(\nabla\times\mathbf{B})}{\mu_0}$ (Dunlop et al., 2002) (h; j_L, j_M and j_N). (i-k) MMS 2 measurements of the electron density (i; n_e), electron velocity in LMN coordinates (j; v_{eL}, v_{eM} and v_{eN}), and ion and electron temperatures (k; T_i and T_e) in the directions parallel ($\|$) and perpendicular ($\perp$) to the local magnetic field. GSM components of the LMN axes are: $\mathbf{L} = (0.955,\ -0.298,\ -0.021)$, $\mathbf{M} = (0.296,\ 0.953,\ -0.059)$, and $\mathbf{N} = (0.038,\ 0.050,\ 0.998)$ (Text S2).

3 Reconstruction of the Electron-scale Current Sheet

We investigate the ECS structure in detail by use of two sophisticated data analysis techniques that can reconstruct multi-dimensional magnetic field structures in regions around the spacecraft from in situ measurements of the magnetic field and plasma bulk parameters. One is a single-spacecraft method based on electron-magnetohydrodynamics (EMHD) equations that can recover quasi-steady, two-dimensional (2-D) magnetic, electrostatic, and electron velocity fields around the path of the observing spacecraft, hereafter called EMHD reconstruction (Sonnerup et al., 2016; Text S4). The other is a multi-spacecraft method based on polynomial (second-order Taylor) expansion of the magnetic field that can recover three-dimensional (3-D) magnetic field using instantaneous measurements by the four spacecraft of the magnetic field and particle current density, called polynomial reconstruction (Denton et al., 2020; Text S5).

To analyze the dimensionality of the ECS, the Maximum Directional Derivative (MDD) method (Shi et al., 2019) was applied to four-spacecraft measurements of the magnetic field for an interval 12:18:29–12:18:37 UT surrounding the reconstruction interval (Figure 3). Figure 3e,f shows that the maximum eigenvalue is much larger than the other two eigenvalues and the first dimension number index D_1 (Rezeau et al., 2018) is much larger than the other two indices, suggesting that the magnetic structure of the ECS was locally nearly 1-D during the reconstruction interval. Figure 3g shows that $\mathbf{k}_{\max}$, which can be taken as the ECS normal direction, was stably northward throughout the reconstruction interval. These results indicate that the ECS was approximately planar with no significant undulation on the scale of the spacecraft separation ~18 km which was comparable to the electron inertial length ($d_e \sim 14$ km). It is also seen that the 2-D assumption made in the EMHD reconstruction is well satisfied in this nearly 1-D ECS.

Figures 2e-2k show the magnetic field and plasma data from MMS, used as input for the two reconstruction techniques, in a current-sheet ('LMN') coordinate system (Text S2): the current-sheet normal points along $\mathbf{N}$ (roughly northward in the magnetotail), the reconnecting antiparallel magnetic field component is along $\mathbf{L}$ (roughly sunward), and $\mathbf{M} = \mathbf{N} \times \mathbf{L}$ is along the 'X-line' direction (roughly duskward). A weak guide field (~2 nT) (Zhou et al., 2019), the compo-

nent (B_M) along the X-line of the magnetic field external to the entire larger-scale current sheet or, in this case, at the center of the ECS (Figure 2f), confirms that reconnection occurred under nearly antiparallel magnetic field conditions. Negative to positive variations of B_N (Figure 2g) is consistent with MMS moving from the anti-sunward to sunward side of the reconnection site; the X-line was moving anti-sunward (Text S3). The assumptions of constant density and constant and isotropic electron temperature made in the EMHD reconstruction are approximately satisfied for an intense current density interval at 12:18:32.1–12:18:34.0 UT (Figure 2i,k), to which the method is applied.

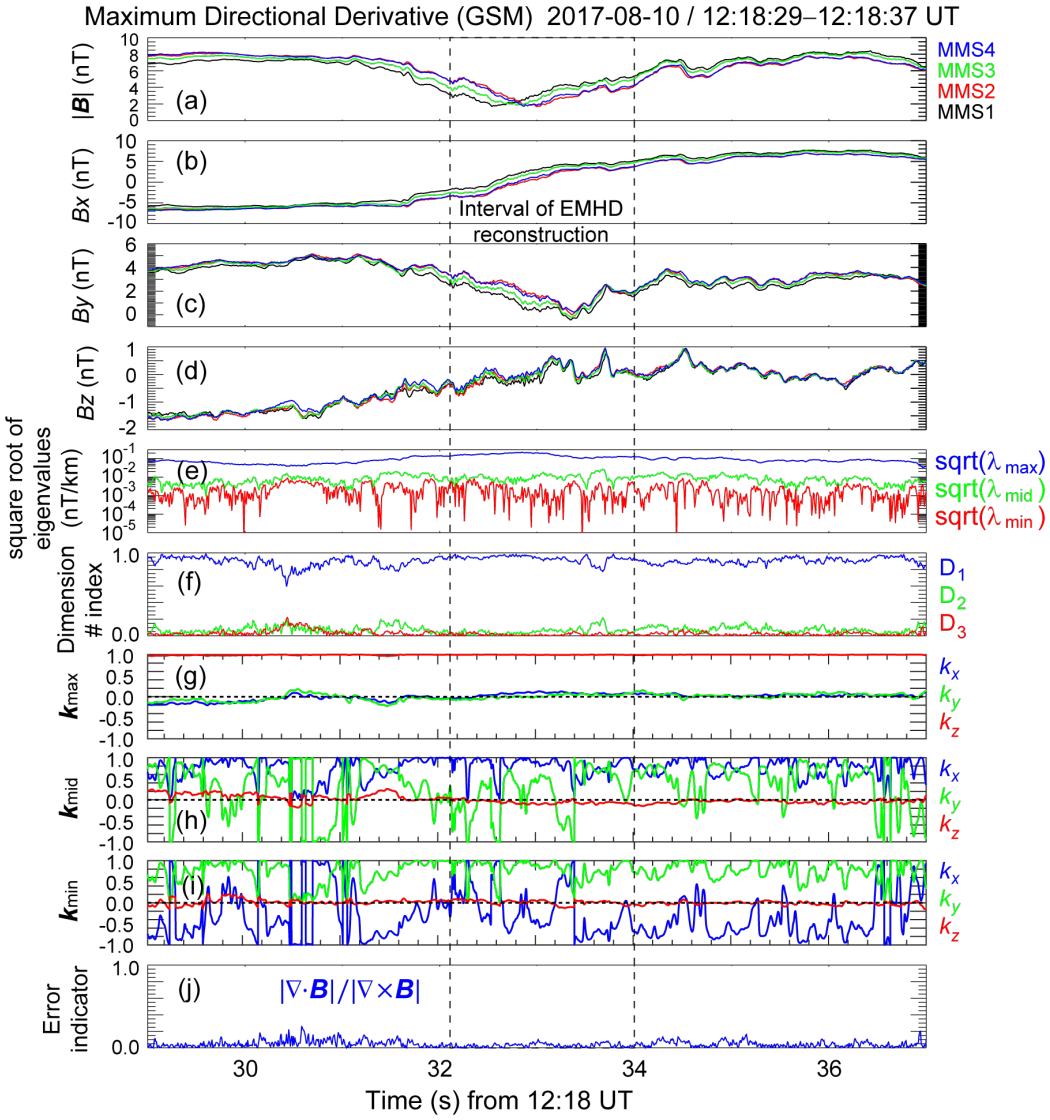

Figure 3. Results from the MDD method (Shi et al., 2019) applied to an interval 12:18:29–12:18:37 UT. (a-d) GSM components of the magnetic field measured by the four MMS spacecraft (a; $|\mathbf{B}|$, b; B_x, c; B_y, d; B_z). (e) Square roots of the maximum, intermediate, and minimum eigenvalues ($\lambda_{\rm max}$, $\lambda_{\rm mid}$, $\lambda_{\rm min}$) of the 3×3 MDD matrix (Shi et al., 2019). (f) Dimension number indices (Rezeau et al., 2018), defined as $D_1 = \frac{(\lambda_{\rm max}-\lambda_{\rm mid})}{\lambda_{\rm max}}$, $D_2 = \frac{(\lambda_{\rm mid}-\lambda_{\rm min})}{\lambda_{\rm max}}$, and $D_3 = \frac{\lambda_{\rm min}}{\lambda_{\rm max}}$, that can be used as measures of the dimensionality of the structure encountered by the spacecraft. (g-i) Eigenvectors corresponding to the three eigenvalues (g; $\mathbf{k}_{\rm max}$, h; $\mathbf{k}_{\rm mid}$, i; $\mathbf{k}_{\rm min}$). (j) $\frac{|\nabla \bullet \mathbf{B}|}{|\nabla \times \mathbf{B}|}$ as an error proxy.

Both the EMHD and polynomial reconstruction results (Figures 4a-4d and 4f-4i) clearly show that an electron-scale magnetic island was forming and growing in the ECS with a thickness of about one d_e. This is consistent with the MDD result suggesting that the ECS had a planar and elongated configuration (Figure 3), ideal for island generation (Daughton et al., 2006). Figures 4a-4d show that over a ~0.4 s interval of 12:18:32.6–12:18:33.0 UT, during which the current sheet was crossed in the order of MMS 1, MMS 3, MMS 4, and MMS 2 (Figure 2e), both the length (along $\mathbf{L}$) and width (along $\mathbf{N}$) of the island grew. An entirely consistent feature is seen in Figures 4f-4i. We also note that the time scale (~0.4) of the ECS crossing is comparable to the proton cyclotron period, so that the island growth was in fact slow on the electron time scale; the quasi-steady assumption of the EMHD reconstruction is approximately satisfied. Furthermore, the energy-conversion rate $\mathbf{j} \bullet \mathbf{E}^{'} = \mathbf{j}_p \bullet (\mathbf{E}+\mathbf{v}_e \times \mathbf{B})$ (Zenitani et al., 2011) (Figure 4e), where the particle current density is $\mathbf{j}_p = en_e\,(\mathbf{v}_i - \mathbf{v}_e)$ with the elementary charge of e and $\mathbf{E}$ the electric field measured in the spacecraft frame, is strongly positive around an X-point closer to the center of the reconstruction domain. Its magnitude (~0.5 nW m^{-3}) is comparable to the value (~0.2 nW m^{-3}) expected for fast reconnection, based on the current density ~150 nA m^{-2} (Figure 2h) and reconnection electric field ~1.3 mV m^{-1} for $B \approx 15$ nT and inflow ion speed of $\sim 0.1 V_{\rm iA} \approx 85$ km s^{-1} (Figure 2b). We thus conclude that energy conversion at the X-point was ongoing. Note that the active X-point was captured inside the MMS tetrahedron during the ECS crossing (Figures 4a-4d, 4g, and 4h), reinforcing the conclusions based on the reconstruction results.

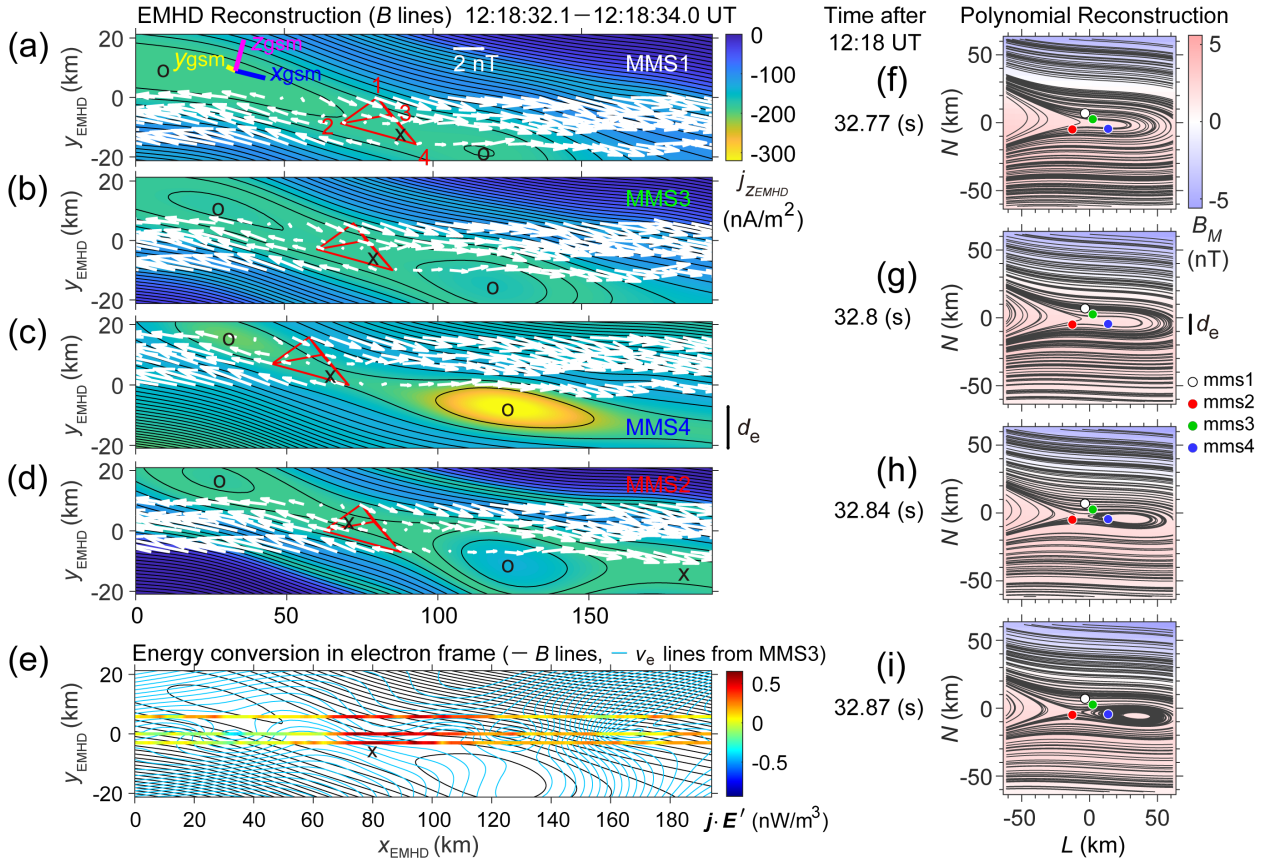

Figure 4. Magnetic fields recovered from the two reconstruction methods (Texts S4 and S5). (a-d) 2-D magnetic fields from the EMHD reconstruction (Sonnerup et al., 2016) using the data taken at 12:18:32.1–12:18:34.0 UT individually for each of the four spacecraft, shown in the order of current sheet crossing (MMS 1, a; MMS 3, b; MMS 4, c; then MMS 2, d; as seen in Figure 2e). Black curves show the reconstructed magnetic field-lines, colors the out-of-plane component ($j_{z,EMHD}$) of the reconstructed current density, and white arrows the projections onto the reconstruction (x_{EMHD}–y_{EMHD}) plane of the measured magnetic fields along the paths of the four spacecraft. The bars near the upper-left corner of panel (a) are the projections of the unit GSM axes (blue, $\hat{\mathbf{x}}_{\mathrm{GSM}}$; yellow, $\hat{\mathbf{y}}_{\mathrm{GSM}}$; magenta, $\hat{\mathbf{z}}_{\mathrm{GSM}}$). (e) Magnetic field lines (black curves) and electron streamlines (blue curves) reconstructed from the MMS 3 data, with $\mathbf{j}_p \bullet \mathbf{E}'$ (Zenitani et al., 2011) measured along the paths of MMS 1, MMS 2, and MMS 3 in color. (f-i) Projection onto the L–N plane of 3-D magnetic field-lines reconstructed using the polynomial reconstruction (Denton et al., 2020) from instantaneous measurements by the four spacecraft of $\mathbf{B}$ and $\mathbf{j}_p$, with reconstructed B_M in color.

In order to reveal how fast the magnetic island was growing, we calculated the amount of magnetic flux per unit length along **M** embedded between the reconstructed X- and O-points closer to the center of the reconstruction domain. Consistent with the island growth, the flux increases with time (Figure 5a) and the measured component of the electric field along **M** (E_M) appears to vary in space and time (Figure 5c). However, the estimated rates of flux accumulation inside the island (Figure 5b) are about one order of magnitude smaller than the measured E_M (flux injection rate) that is comparable to the expected reconnection electric field of ~1.3 mV m^{-1}. Tests of our reconstruction methods using simulated data show that the estimated fluxes may differ by a factor of 4 at most (Figure S3 and Texts S4 and S5). Thus, the result suggests that the in-plane magnetic field injected into the ECS was mostly annihilated, rather than ejected out of the X-point into the island, at the time and portion of the ECS observed by MMS.

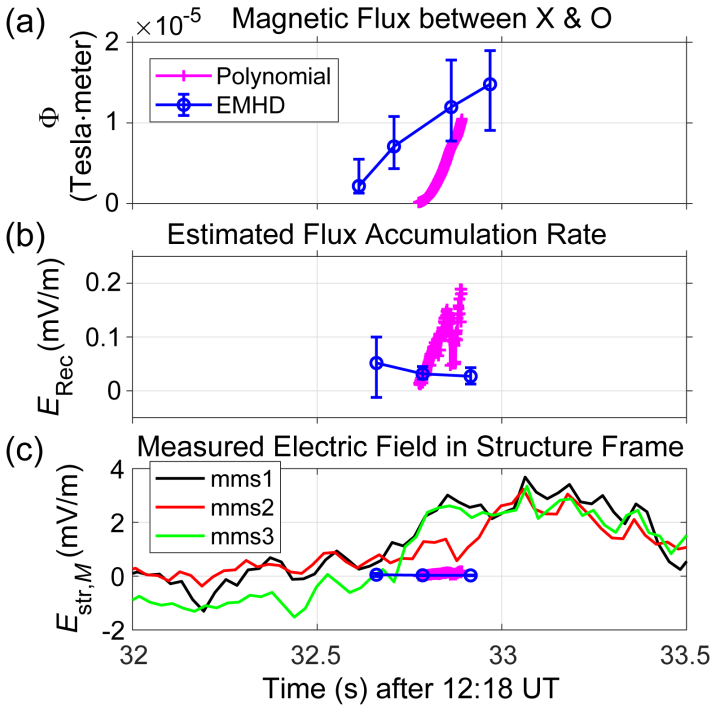

Figure 5. Reconnection electric fields, estimated from the EMHD and polynomial reconstructions, compared with the measured electric field. (a) In-plane magnetic flux (Φ) embedded between the X- and O-points around the center of the reconstruction domain as a function of time which is defined as that of the current sheet crossing ($B_L = 0$) for the EMHD reconstruction. (b) Rate of flux accumulation inside the island ($E_{\mathrm{Rec}} = \frac{\partial \Phi}{\partial t}$). (c) M component ($E_{str,M}$) of the electric field from MMS 1, MMS 2, and MMS 3 that made reliable electric field measurements, transformed into the frame comoving with the structure

(see Text S3 for details), along with E_{Rec}. The upper and lower levels of the error bars are based on results from the EMHD reconstructions with an offset of $B_z = +0.1$ nT or -0.1 nT in GSE added to the measurements, considering that the error in the magnetic field measurements is ~0.1 nT (Russell et al., 2016). The flux values from the polynomial reconstruction are shown only when both the X- and O-points are within twice the spacecraft separation of the centroid of the MMS spacecraft (Denton et al., 2021).

4 Theoretical analysis

Is fast annihilation of the magnetic field as detected by MMS physically possible in an ECS? For quasi-steady 2-D reconnection in collisionless plasmas, electron demagnetization (violation of the electron frozen-in condition) at the X-line occurs when off-diagonal terms of the electron pressure tensor are significant (Hesse et al., 2011). Consistently, nongyrotropic electron velocity distributions as a manifestation of electron demagnetization have been observed in the present (Li et al., 2019) as well as other EDRs (Burch et al., 2016; Torbert et al., 2018). Earlier studies also demonstrated that the nongyrotropic electron pressure term can quantitatively account for the electric field (E_M) of fast reconnection as observed (Egedal et al., 2019). Our theoretical analysis shows that when the generalized Ohm's law has a term equivalent to the nongyrotropic electron pressure tensor and the ECS is elongated in the exhaust direction, a diffusion equation for B_L (Eq. (S7)),

$$\frac{\partial B_L}{\partial t} \approx r_{\mathrm{ge}} V_\infty \frac{\partial^2 B_L}{\partial N^2}, \quad (1)$$

is applicable, where r_{ge} is the gyroradius of thermal electrons and V_∞ is the electron inflow speed ($|v_{eN}|$) immediately outside of the EDR (Text S7). This equation is supported by a solution of the EMHD equations (Figure S7) and is consistent with the observed fast annihilation (Text S7). The fast collisionless annihilation is in stark contrast with the classic (resistive magnetohydrodynamics) model (Parker, 1957; Sweet, 1958) of reconnection in an elongated current sheet in which the annihilation is negligibly small under magnetotail conditions. However, we do not exclude a likely possibility that at around the sunward and anti-sunward ends of the present ECS, where the magnetic field may have a Y-type geometry (Figure 1b,c), the magnetic field was efficiently reconnected and ejected downstream, as observed for other magnetotail reconnection events (Nakamura et al., 2018).

5 Conclusions

The main results of our study can be summarized as follows. (1) The MMS observations reported in the present letter are consistent with fast energy conversion in an elongated EDR dominated by magnetic field annihilation; (2) the fully kinetic simulation shows annihilation-dominated energy conversion in and around electron-scale islands formed in the EDR elongated in the exhaust direction (Figure 1e,f); and (3) theoretical analysis suggests fast collisionless magnetic diffusion in a planar EDR with nongyrotropic electrons (Text S7). Thus,

three different approaches, namely, our MMS event analysis, simulation, and theoretical analysis all support magnetic field annihilation in an elongated EDR. The discovery of the annihilation in a reconnecting ECS could have far-reaching implications for how magnetic energy is dissipated in plasma turbulence in the collisionless regime, because reconnection has been suggested to play a role in the dissipation process (Matthaeus and Lamkin, 1986; Retinò et al., 2007; Servidio et al., 2009).

An important question remains about whether the magnetic energy dissipated by the annihilation is partitioned to thermal or nonthermal electrons, if not to the electron bulk flow. Recently, Nakamura et al. (2021) have shown, based on a fully kinetic simulation, that electrons are strongly heated in electron-scale magnetic islands where the annihilation is ongoing. In the present event, however, no clear signature of electron heating or energization was found likely because electron beta outside the EDR was so high (~5) that available magnetic energy was probably too small for energization effects to be identified; even if all the magnetic energy was converted to electron thermal energy, the temperature increase would be only about 20% of the ambient value. It is noted that for typical reconnection, only ~2% of the available magnetic energy is partitioned to thermal electrons in reconnection exhausts (Phan et al., 2013). Thus, the process of energy partition through the annihilation will need to be quantitatively assessed in the future.

Acknowledgments, and Data

All MMS data used in this study are publicly available via the MMS Science Data Center at https://lasp.colorado.edu/mms/sdc/public/. All code used to analyze the MMS data in this study is based on the publicly available SPEDAS tools (Angelopoulos et al., 2019) (http://spedas.org/blog/), except for the Matlab code for the EMHD and polynomial reconstructions. The Matlab code for the EMHD reconstruction can be found at the Zenodo (https://doi.org/10.5281/zenodo.3900642), and that for the polynomial reconstruction at https://doi.org/10.5281/zenodo.3906853. H.H. thanks W. Daughton for discussions. We are grateful for the dedicated efforts of the MMS team. For the simulation reported in this paper, we acknowledge PRACE for awarding us access to MareNostrum at the Barcelona Supercomputing Center (BSC), Spain. The work by H.H. was supported by JSPS Grant-in-aid for Scientific Research KAKENHI 21K03504. R.E.D was supported by a NASA grant (80NSSC19K0254). T.K.M.N. was supported by the Austrian Research Fund (FWF) P32175-N27.

References

Angelopoulos, V., McFadden, J. P., Larson, D., et al. (2008). Tail reconnection triggering substorm onset. *Science*, *321*, 931–935.

Angelopoulos, V., Cruce, P., Drozdov, A., et al. (2019). The Space Physics Environment Data Analysis System (SPEDAS). *Space Sci. Rev.*, *215*, 9. https://doi.org/10.1007/s11214-018-0576-4.

Burch, J. L., Torbert, R. B., Phan, T. D., et al. (2016). Electron-scale measurements of magnetic reconnection in space. *Science*, *352*, aaf2939. doi:10.1126/science.aaf2939.

Daughton, W., Scudder, J., & Karimabadi, H. (2006). Fully kinetic simulations of undriven magnetic reconnection with open boundary conditions. *Phys. Plasmas*, *13*, 072101. https://doi.org/10.1063/1.2218817.

Denton, R. E., Sonnerup, B. U. Ö., Hasegawa, H., et al. (2016). Motion of the MMS spacecraft relative to the magnetic reconnection structure observed on 16 Oct 2015 at 1307 UT. *Geophys. Res. Lett.*, *43*, 5589–5596. doi:10.1002/2016GL069214.

Denton, R. E., Sonnerup, B. U. Ö., Russell, C. T., et al. (2018). Determining L-M-N current sheet coordinates at the magnetopause from Magnetospheric Multiscale data. *J. Geophys. Res. Space Physics*, *123*, 2274–2295. https://doi.org/10.1002/2017JA024619.

Denton, R. E., Torbert, R. B., Hasegawa, H., et al. (2020). Polynomial reconstruction of the reconnection magnetic field observed by multiple spacecraft. *J. Geophys. Res. Space Physics*, *125*, e2019JA027481. https://doi.org/10.1029/2019JA027481.

Denton, R. E., Torbert, R. B., Hasegawa, H., et al. (2021). Two-dimensional velocity of the magnetic structure observed on 11 July 2017 by the Magnetospheric Multiscale spacecraft, *J. Geophys. Res. Space Physics*, *126*, e2020JA028705, https://doi.org/10.1029/2020JA028705.

Dunlop, M. W., Balogh, A., Glassmeier, K.-H., & Robert, P. (2002). Four-point Cluster application of magnetic field analysis tools: The Curlometer. *J. Geophys. Res.*, *107*, 1384. doi:10.1029/2001JA005088.

Egedal, J., Ng, J., Le, A., et al. (2019). Pressure tensor elements breaking the frozen-in law during reconnection in Earth's magnetotail. *Phys. Rev. Lett.*, *123*, 225101. doi:10.1103/PhysRevLett.123.225101.

Ergun, R. E., Tucker, S., Westfall, J., et al. (2016). The axial double probe and fields signal processing for the MMS mission. *Space Sci. Rev.*, *199*, 167–188. doi:10.1007/s11214-014-0115-x.

Fujimoto, K. (2006). Time evolution of the electron diffusion region and the reconnection rate in fully kinetic and large system. *Phys. Plasmas*, *13*, 072904.

Hasegawa, H., Sonnerup, B. U. Ö., Denton, R. E., et al. (2017). Reconstruction of the electron diffusion region observed by the Magnetospheric Multiscale spacecraft: First results. *Geophys. Res. Lett.*, *44*, 4566–4574. doi:10.1002/2017GL073163.

Hasegawa, H., Denton, R. E., Nakamura, R., et al. (2019). Reconstruction of the electron diffusion region of magnetotail reconnection seen by the MMS

spacecraft on 11 July 2017. *J. Geophys. Res. Space Physics*, *124*, 122–138. https://doi.org/10.1029/2018JA026051.

Hasegawa, H., Nakamura, T. K. M., Denton, R. E. (2021). Reconstruction of the electron diffusion region with inertia and compressibility effects. *J. Geophys. Res. Space Physics*, submitted, https://doi.org/10.1002/essoar.10507704.1.

Hesse, M., Neukirch, T., Schindler, K., Kuznetsova, M., & Zenitani, S. (2011). The diffusion region in collisionless magnetic reconnection. *Space Sci. Rev.*, *160*, 3–23. doi:10.1007/s11214-010-9740-1.

Kawano, H., & Higuchi, T. (1995). The bootstrap method in space physics: Error estimation for minimum variance analysis. *Geophys. Res. Lett.*, *22*, 307–310. doi:10.1029/94GL02969.

Kuznetsova, M. M., Hesse, M., Rastaetter, L., et al. (2007). Multiscale modeling of magnetospheric reconnection, *J. Geophys. Res.*, *112*, A10210. doi:10.1029/2007JA012316.

Li, X., Wang, R., Lu, Q., et al. (2019). Observation of nongyrotropic electron distribution across the electron diffusion region in the magnetotail reconnection. *Geophys. Res. Lett.*, *46*, 14263–14273. https://doi.org/10.1029/2019GL085014.

Lindqvist, P.-A., Olsson, G., Torbert, R. B., et al. (2016). The Spin-plane Double Probe electric field instrument for MMS. *Space Sci. Rev.*, *199*, 137–165. doi:10.1007/s11214-014-0116-9.

Liu, Y.-H., Hesse, M., Guo, F., et al. (2017). Why does steady-state magnetic reconnection have a maximum local rate of order 0.1? *Phys. Rev. Lett.*, *118*, 085101. doi:10.1103/PhysRevLett.118.085101.

Matthaeus, W. H., & Lamkin, S. L. (1986). Turbulent magnetic reconnection. *Phys. Plasmas*, *29*(8), 2513–2534. https://doi.org/10.1063/1.866004.

Nagai, T., Shinohara, I., Fujimoto, M., et al. (2001). Geotail observations of the Hall current system: Evidence of magnetic reconnection in the magnetotail. *J. Geophys. Res.*, *106*, 25929–25949.

Nagai, T., Shinohara, I., Fujimoto, M., Matsuoka, A., Saito, Y., & Mukai, T. (2011). Construction of magnetic reconnection in the near-Earth magnetotail with Geotail. *J. Geophys. Res.*, *116*, A04222. doi:10.1029/2010JA016283.

Nakamura, T. K. M., Genestreti, K. J., Liu, Y.-H., et al. (2018). Measurement of the magnetic reconnection rate in the Earth's magnetotail. *J Geophys. Res. Space Physics*, *123*, 9150–9168. https://doi.org/10.1029/2018JA025713.

Nakamura, T. K. M., Stawarz, J. E., Hasegawa, H., Narita, Y., Franci, L., Wilder, F. D. et al. (2020). Effects of fluctuating magnetic field on the growth of the Kelvin-Helmholtz instability at the Earth's magnetopause. *Journal of Geophysical Research: Space Physics*, *125*, e2019JA027515. https://doi.org/10.1029/2019JA027515.

Nakamura, T. K. M., Hasegawa, H., Genestreti, K. J., Denton, R. E., Phan, T. D., Stawarz, J. E., et al. (2021). Fast cross-scale energy transfer during turbulent magnetic reconnection. *Geophysical Research Letters*, *48*, e2021GL093524. https://doi.org/10.1029/2021GL093524.

Øieroset, M., Phan, T. D., Fujimoto, M., Lin, R. P., & Lepping, R. P. (2001). In situ detection of collisionless reconnection in the Earth's magnetotail. *Nature*, *412*, 414–417.

Parker, E. N. (1957). Sweet's mechanism for merging magnetic fields in conducting fluids. *J. Geophys. Res.*, *62*, 509–520.

Phan, T. D., Shay, M. A., Gosling, J. T., et al. (2013). Electron bulk heating in magnetic reconnection at Earth's magnetopause: Dependence on the inflow Alfven speed and magnetic shear. *Geophys. Res. Lett.*, *40*, 4475–4480. doi:10.1002/grl.50917.

Pollock, C., Moore, T., Jacques, A., et al. (2016). Fast plasma investigation for Magnetospheric Multiscale. *Space Sci. Rev.*, *199*, 331–406. doi:10.1007/s11214-016-0245-4.

Retinò, A., Sundkvist, D., Vaivads, A., Mozer, F., André, M., & Owen, C. J. (2007). In situ evidence of magnetic reconnection in turbulent plasma. *Nature Physics*, *3*, 235–238. doi:10.1038/nphys574.

Rezeau, L., Belmont, G., Manuzzo, R., Aunai, N., & Dargent, J. (2018). Analyzing the magnetopause internal structure: New possibilities offered by MMS tested in a case study. *J. Geophys. Res. Space Physics*, *123*, 227–241. https://doi.org/10.1002/2017JA024526.

Russell, C. T., Anderson, B. J., Baumjohann, W., et al. (2016). The Magnetospheric Multiscale Magnetometers, *Space Sci. Rev.*, *199*, 189–256. doi:10.1007/s11214-014-0057-3.

Servidio, S., Matthaeus, W. H., Shay, M. A., Cassak, P. A., & Dmitruk, P. (2009). Magnetic reconnection in two-dimensional magnetohydrodynamic turbulence. *Phys. Rev. Lett.*, *102*, 115003.

Shay, M. A., Drake, J. F., & Swisdak, M. (2007). Two-scale structure of the electron dissipation region during collisionless magnetic reconnection. *Phys. Rev. Lett.*, *99*, 155002. doi:10.1103/PhysRevLett.99.155002.

Shi, Q. Q., Tian, A. M., Bai, S. C., et al. (2019). Dimensionality, coordinate system and reference frame for analysis of in-situ space plasma and field data. *Space Sci. Rev.*, *215*, 35. https://doi.org/10.1007/s11214-019-0601-2.

Sonnerup, B. U. Ö., & Scheible, M. (1998). Minimum and maximum variance analysis, in *Analysis Methods for Multi-Spacecraft Data*, G. Paschmann, P. W. Daly, Eds., ISSI/ESA, chap. 8, pp. 185–220.

Sonnerup, B. U. Ö., Hasegawa, H., Denton, R. E., & Nakamura, T. K. M. (2016). Reconstruction of the electron diffusion region. *J. Geophys. Res. Space Physics*,

121, 4279–4290. doi:10.1002/2016JA022430.

Sweet, P. A. (1958). The neutral point theory of solar flares, in *Electromagnetic Phenomena in Cosmical Physics*, B. Lehnert, Ed., Cambridge, pp. 123–134.

Torbert, R. B., Russell, C. T., Magnes, W., et al. (2016). The FIELDS instrument suite on MMS: scientific objectives, measurements, and data products. *Space Sci. Rev.*, *199*, 105–135. doi:10.1007/s11214-014-0109-8.

Torbert, R. B., Burch, J. L., Phan, T. D., et al. (2018). Electron-scale dynamics of the diffusion region during symmetric magnetic reconnection in space. *Science*, *362*, 1391–1395. doi:10.1126/science.aat2998.

Torbert, R. B., Dors, I., Argall, M. R., et al. (2020). A new method of 3-D magnetic field reconstruction. *Geophys. Res. Lett.*, *47*, e2019GL085542. https://doi.org/10.1029/2019GL085542.

Zenitani, S., Hesse, M., Klimas, A., & Kuznetsova, M. (2011). New measure of the dissipation region in collisionless magnetic reconnection. *Phys. Rev. Lett., 106*, 195003. doi:10.1063/1.3554655.

Zhou, M., Deng, X. H., Z. H. Zhong, et al. (2019). Observations of an electron diffusion region in symmetric reconnection with weak guide field. *Astrophys. J.*, *870*, 34. https://doi.org/10.3847/1538-4357/aaf16f.